Effect of bio-tissue deformation behavior due to intratumoral injection on magnetic hyperthermia

Yundong Tang(汤云东)[1,†], Jian Zou(邹建)[1], Rodolfo C.C. Flesch[2], and Tao Jin(金涛)[3]

[1] *College of Physics and Information Engineering, Fuzhou University, Fuzhou* 350116, *China*
[2] *Departamento de Automação e Sistemas, Universidade Federal de Santa Catarina,* 88040-900 *Florianópolis, SC, Brazil*
[3] *College of Electrical Engineering and Automation, Fuzhou University, Fuzhou* 350108, *China*

(Received 7 March 2022; revised manuscript received 10 May 2022; accepted manuscript online 29 May 2022)

Thermal damage of malignant tissue is generally determined not only by the characteristics of bio-tissues and nanoparticles but also the nanofluid concentration distributions due to different injection methods during magnetic hyperthermia. The latter has more advantages in improving the therapeutic effect with respect to the former since it is a determining factor for the uniformity of nanofluid concentration distribution inside the tumor region. This study investigates the effect of bio-tissue deformation due to intratumoral injection on the thermal damage behavior and treatment temperature distribution during magnetic hyperthermia, in which both the bio-tissue deformation due to nanofluid injection and the mass diffusion after injection behavior are taken into consideration. The nanofluid flow behavior is illustrated by two different theoretical models in this study, which are Navier–Stokes equation inside syringe needle and modified Darcy's law inside bio-tissue. The diffusion behavior after nanofluid injection is expressed by a modified convection–diffusion equation. A proposed three-dimensional liver model based on the angiographic data is set to be the research object in this study, in which all bio-tissues are assumed to be deformable porous media. Simulation results demonstrate that the injection point for syringe needle can generally achieve the maximum value in the tissue pressure, deformation degree, and interstitial flow velocity during the injection process, all of which then drop sharply with the distance away from the injection center. In addition to the bio-tissue deformation due to injection behavior, the treatment temperature is also highly relevant to determine both the diffusion duration and blood perfusion rate due to the thermal damage during the therapy.

Keywords: tissue deformation, thermal apoptosis analysis, heat transfer, mass transfer

PACS: 44.10.+i, 44.05.+e, 87.85.J– **DOI:** 10.1088/1674-1056/ac744c

1. Introduction

Magnetic hyperthermia has been considered to be a promising therapeutic method due to its low side effects and less trauma in recent years.[1–3] The most important factor for the success of therapy is to control the treatment temperature for tumor region within a range from 42 °C to 46 °C, in which malignant cells can be damaged due to their thermal sensitivity while healthy cells can survive.[4,5] However, the treatment temperature distribution inside the tumor region should be determined by many factors, and the most two important elements are the power dissipation for magnetic nanoparticles (MNPs) and the nanofluid concentration distribution inside the tumor region.[6,7] The heat dissipated by the MNPs is primarily determined by the characteristics of the applied magnetic field and MNPs.[8,9] The concentration distribution depends on the delivery approaches for nanofluid, which can generally be intratumoural injection and systematic delivery.[10] The intratumoural injection was usually considered in previous studies since it can obtain a high concentration of MNPs inside the malignant tissue.[11,12]

Although magnetic nanofluid hyperthermia has received widespread attention from a large number of researchers, the delivery behavior for nanofluid still lack enough concerns in previous literature. Most of previous reports just assumed the MNPs inside the tumor region to have a homogeneous distribution or just to be an MNP core in order to simplify their model.[13] However, these approaches are greatly far away from a real practice. Astefanoaei *et al.* simulated the behavior for MNPs transport inside the bio-tissue by considering the extension of Darcy's equation, and also investigated the effect of naofluid flow rate on the treatment temperature of tumor region.[14,15] Nevertheless, a spherical-shape nanofluid concentration distribution with center in the injection site was considered, which is not very likely to be observed in clinical practice. LeBrun *et al.* generated directly the specific absorption rate distribution by developing the computer algorithms for given micro computed tomography images in order to improve the accuracy for treatment temperature during hyperthermia.[16] This study ignored the heat generation behavior for MNPs, which is relevant to the nanofluid concentration distribution, the MNPs, and magnetic field. Thus, one cannot optimize the treatment temperature distribution for tumor region by regulating these influencing factors for a clinical application. There were also previous reports that focused on the effect of infusion parameters on the treatment temperature distribution, in which the local displacements of bio-tissue due

[†]Corresponding author. E-mail: tangyundong@fzu.edu.cn

© 2023 Chinese Physical Society and IOP Publishing Ltd

to nanofluid injection were considered in the optimization for nanofluid dose.[17] Further, this study can just present the analysis results for a single point inside the tumor region since the analytical solution was used in the analysis process for a proposed geomentric model. The similar approaches were also considered in several previous literature.[18] Singh *et al.* revealed the local thermal damage during the therapy can vary the porosity for bio-tissue and the diffusion rate for nanofluid, which can further promote the nanofluid flow from a higher concentration to a lower case.[19] However, the nanofluid concentration due to the injection behavior was not discussed in this study.

This paper investigates the treatment temperature distribution for a proposed geometric model by considering the concentration distribution due to nanofluid injection behavior, in which the bio-tissue properties change with the bio-tissue deformation due to nanofluid injection process. During this injection process, the nanofluid flow is described by the Navier–Stokes equation inside the syringe needle, and is illustrated by the modified Darcy's law inside the bio-tissue. In addition to the injection behavior, the diffusion behavior after nanofluid injection is also taken consideration for the bio-tissue damage. All these analytic methods are based on a reconstructed liver model in this study, which comes from a real clinical image. Although all the calculations are carried out by considering a three-dimensional model, all results in this paper are shown in one-dimension or two-dimension to have a better presentation. Finite element method is used to solve partial differential equations for the concentration and therapeutic temperature distribution inside the bio-tissue during magnetic hyperthermia, in which the initial and boundary conditions should be given for the proposed geometric model.

2. Theoretical framework

2.1. Geometric model

A three dimensional liver model proposed by this study is reconstructed by considering an open-source medical image processing software, 3D Slicer, in which the input image comes from the abdominal angiography for an adult male. Further, a tumor model is modeled inside this reconstructed liver model after proper mesh simplification in a finite element analysis software. Figure 1(a) shows the views of different directions for the proposed model, while Fig. 1(b) presents its slice view for the x–z plane. For the convenience of comparative analysis, the model proposed in this study takes the tumor center as the coordinate origin. As illustrated in Fig. 1, the proposed liver model has a horizontal diameter of 250 mm, a vertical diameter of 150 mm, and an anteroposterior diameter of 260 mm. The tumor is designed to an ellipsoid shape with a polar radius of 15 mm and two sane equatorial radii of 10 mm. The Fe_3O_4 nanofluid is injected into tumor tissue along a cylindrical syringe, which has an inner radius of 0.4 mm in this study.

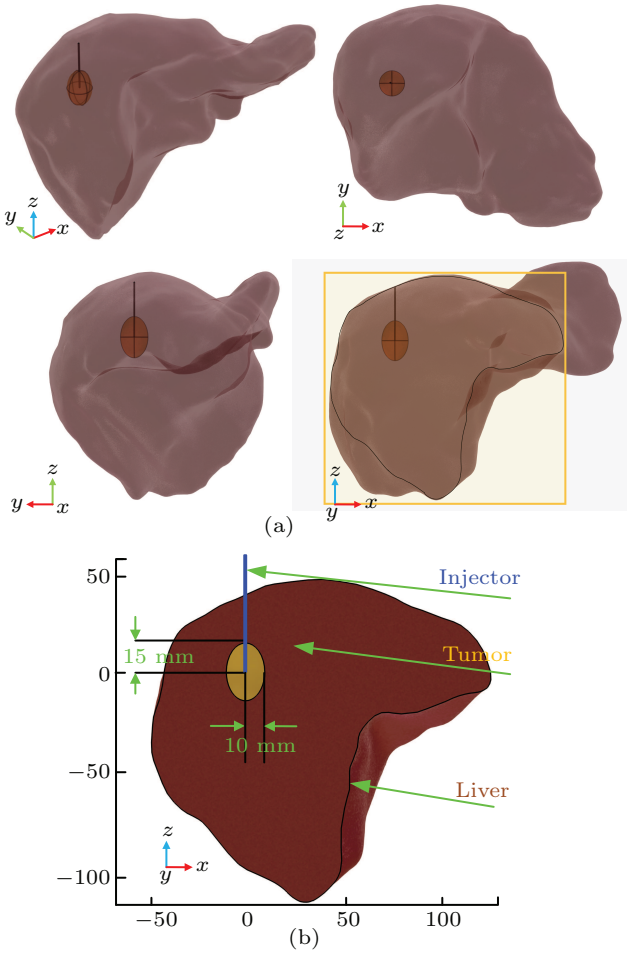


Fig. 1. Proposed three-dimensional geometric model: (a) views of different directions; (b) slice view in xz direction. Axes are in units of mm.

2.2. Bio-tissue deformable model

The injection behavior can result in the local dilatation on bio-tissue due to the action of external pressure, which can then change the internal pressure and stress distribution for the bio-tissue. This study assumes the local dilatation inside tumor is a quasi-static deformation process with small inertial force. An equilibrium state will ultimately be reached between the internal pressure and the external force, which can be illustrated by the Newton's second law[20]

$$\sigma_{lm,m} + F_l = 0, \quad (l, m = x, y \quad \text{or} \quad z), \tag{1}$$

where subscripts l and m refer to the x, y or z coordinates in cartesian space. σ_{lm} denotes the component of the total stress tensor, while $\sigma_{lm,m}$ indicates the divergence of σ_{lm} in the m direction. The effect of gravity on the tissue deformation is ignored in this study, which leads to the zero setting in the component of unit volume force, F_l. This study assumes the biological tissue to be an incompressible porous material, so

an isotropic linear elasticity can be used to approximate the relationship between the mechanical stress and the tissue strain under small deformation[21,22]

$$\varepsilon_{lm} = \frac{1}{E}(\sigma_{lm} - \beta P\delta_{lm} - v(\sigma_{nn}\delta_{lm} - \sigma_{lm} - \beta P\delta_{lm})), \quad (2)$$

where the variable $\sigma_{nn} = \sigma_{xx} + \sigma_{yy} + \sigma_{zz}$ indicates the first stress invariant. The Kronecker function δ_{lm} in Eq. (2) has a further expression as following:

$$\delta(l,m) = \begin{cases} 1, & l = m, \\ 0, & l \neq m. \end{cases} \quad (3)$$

The effective stress coefficient, β, can be expressed as

$$\beta = 1 - \frac{E}{3K_s(1-2v)}. \quad (4)$$

Furthermore, the strain ε_{lm} can also be described by considering tissue displacement[23] as

$$\varepsilon_{lm} = \frac{1}{2}(\nabla \boldsymbol{u} + (\nabla \boldsymbol{u})^{\mathrm{T}}), \quad (5)$$

where $\boldsymbol{u}$ refers to the average displacement of the tissue during the nanofluid injection. The displacement u_z along the z axis is set to be zero in the internal surface of the solid domain, while it will change freely along the x axis and y axes. In addition, the permeability and porosity of the bio-tissue will change with the pore pressure and the volumetric strain when the nanofluid is injected into the tumor tissue by the syringe needle. Thus, one can obtain the functional relationship between the porosity and the pore pressure approximately by a linear and nonlinear equation[24]

$$\phi = \frac{\phi_0 + e}{1 + e}, \quad (6)$$

where variable e is the expansion coefficient of bio-tissue, which is generally used to describe the deformation degree of bio-tissue with the following expression:[23,24]

$$e = \nabla \cdot \boldsymbol{u}. \quad (7)$$

In addition, the relationship between the porosity and the permeability of bio-tissue obeys the power law[25]

$$\frac{K}{K_0} = \left(\frac{\phi}{\phi_0}\right)^3. \quad (8)$$

2.3. Transport and diffusion model for nanofluid injection

The nanofluid injection behavior in the needle can be considered as an incompressible laminar flow, which can be described by the Navier–Stokes equations including the momentum and continuity equation

$$\frac{\partial \rho_{\mathrm{f}}}{\partial t} + \nabla \cdot (\rho_{\mathrm{f}} \boldsymbol{w}) = 0, \quad (9)$$

$$\rho_{\mathrm{f}}(\boldsymbol{w} \cdot \nabla \boldsymbol{w}) = -\nabla P_i + \mu \nabla^2 \boldsymbol{w} + F, \quad (10)$$

where F is the external force per unit volume, which is set to be zero in the case without any external force but the inherent pressure inside bio-tissue. The nanofluid flow caused by interstitial pressure in bio-tissue can be described by modified Darcy's law when solid matrix in bio-tissue can be regarded as a porous elastic material[17,26]

$$\phi_i \left(\boldsymbol{v}_i - \frac{\partial \boldsymbol{u}}{\partial t}\right) = -K_i \cdot \nabla(\phi_i P_i), \quad (11)$$

where value "1" for subscript i denotes tumor region and value "0" indicates healthy region, respectively. $\boldsymbol{v}_i$ is the average fluid flow rate in interstitial tissue, which can have further expression after combining the fluid source term Ψ_{B} and the sink term Ψ_{L}[27]

$$\nabla \cdot (\phi_i \boldsymbol{v}_i) = \psi_{\mathrm{B}} - \psi_{\mathrm{L}}. \quad (12)$$

The variable Ψ_{B} can be described by Starling's law[28]

$$\psi_{\mathrm{B}} = \frac{L_{\mathrm{p}} S}{V}(P_{\mathrm{b}} - P_i - \sigma_{\mathrm{s}}(\pi_{\mathrm{b}} - \pi_i)), \quad (13)$$

where the osmotic pressure term $\sigma_{\mathrm{s}}(\pi_{\mathrm{b}} - \pi_i)$ is usually set to be zero since it is small enough compared to another term $(P_{\mathrm{b}} - P_i)$.[29] The variable Ψ_L can be illustrated by the following expression based on Kedem–Katchalsky model:[30]

$$\psi_{\mathrm{L}} = \begin{cases} 0, & (\Upsilon \in \Re), \\ \frac{L_{\mathrm{pL}} S_{\mathrm{L}}}{V}(P_{\mathrm{b}} - P_{\mathrm{L}}), & (\Upsilon \notin \Re), \end{cases} \quad (14)$$

where the symbol $\Re$ indicates malignant region.

Furthermore, proper initial and boundary conditions are also proposed in order to obtain the solution for the injection process. The initial concentration is set to be zero for all bio-tissues, and is set to be $C_{\max} = 170\ \mathrm{mg \cdot ml^{-1}}$ for nanofluid before the injection behavior. This initial value for nanofluid concentration is also the same to the maximum value at the injection site. Meanwhile, the needle wall insolates the nanofluid from the bio-tissue during the injection process, which should meet the corresponding boundary condition as $-\boldsymbol{n} \cdot \rho_{\mathrm{nf}} v_i = 0$. The nanofluid flux at the needle tip can be illustrated with the following expression:

$$-\boldsymbol{n} \cdot \rho_{\mathrm{nf}} \boldsymbol{v}_i = (v_{\mathrm{inf}} \cdot \rho_{\mathrm{f}})/A_{\mathrm{needle}}, \quad (15)$$

where the right term in Eq. (15) refers to the nanofluid flux.

Although the nanofluid distribution inside the tumor tissue mostly relies on the injection behavior, the diffusion behavior due to the interstitial pressure and concentration difference should not be ignored during the whole process. Nevertheless, the diffusion behavior can generally be ignored in the injection period with a short time. Thus, this study just considers the effect of injection behavior on nanofluid concentration after the nanofluid injection, which can be depicted by a modified convective–diffusion equation[31]

$$\frac{\partial(\phi_i C_i)}{\partial t} + \nabla \cdot (\boldsymbol{v}_i \phi_i C_i) = \nabla \cdot (D_{\mathrm{eff}} \nabla C_i) - k_{\mathrm{f}} C_i, \quad (16)$$

where the variable $k_f C$ indicates the MNPs product term, and the coefficient k_f has further expression as following:[32]

$$k_f = \frac{3(1-\phi_i)}{2\phi_i d_c}\eta v_i. \tag{17}$$

The nanofluid concentration should be continuity between different boundary of bio-tissue, which can be described by using Neumann boundary condition

$$D_0^* \frac{\partial C_0}{\partial r}\bigg|_{r=R_0} = D_1^* \frac{\partial C_1}{\partial r}\bigg|_{r=R_1}. \tag{18}$$

In addition, this study ignores the diffusion effect due to 30 min of treatment duration since it is relatively short with respect to the diffusion duration after the nanofluid injection. Furthermore, a working magnetic field may also contribute to the change of nanofluid distribution during therapy, which however is not considered in this study due to its complicated mechanism.

2.4. Heat transfer and thermal damage model

Once the nanofluid concentration distribution is established by the injection behavior, one can further predict the therapeutic temperature distribution for bio-tissue by considering Pennes biological heat transfer (PBHT) equation.[33–35] This PBHT equation can be solved by using the finite element method for the proposed geometric model when one obtains the properties for the bio-tissue, magnetic field, and also the MNPs

$$\begin{aligned}\rho_i c_i \frac{\partial T_i}{\partial t} &= \nabla\cdot(k_i \nabla T_i) + \rho_b c_b \omega_b (T_b - T_i) \\ &\quad + Q_{met} + i\cdot Q_{MNP},\end{aligned} \tag{19}$$

where the total power dissipation due to the MNPs, Q_{MNP}, is directly relevant to an individual heat of MNP P_{MNP} and the nanofluid concentration, which have the corresponding expression $Q_{MNP} = P_{MNP}\cdot C_i/\rho_{MNP}$. The concentration C_i is then determined by the volume fraction θ_i and the MNP density ρ as $C_i = \theta_i \cdot \rho_{MNP}$. The individual power dissipation for MNP due to applied magnetic field can be illustrated by Rosensweig theory[36,37]

$$P_{MNP} = \pi\mu_0\chi_0 H_m^2 f \frac{2\pi f\tau_{eff}}{1+(2\pi f\tau_{eff})^2}. \tag{20}$$

The increase in the treatment temperature can result in the thermal damage of malignant cells, which can be illustrated by the Arrhenius damage model.[38,39] The thermal damage Ω in Eq. (21) is determined by many factors, the treatment temperature, the treatment duration, and also the Arrhenius kinetic coefficients including the activation energy E_a and the frequency factor A for the ablation process

$$\Omega(x,y,z,\tau) = A\int_0^\tau \exp\left[\frac{-E_a}{R_u T(x,y,z,t)}\right] d\tau. \tag{21}$$

This thermal damage Ω can further be converted into a new evaluating index, the degree of tissue injury α, which have a value range between "0" with no damage and "1" with a complete damage to tumor cells[40]

$$\alpha(x,y,z,t) = 1 - e^{[-\Omega(x,y,z,\tau)]}. \tag{22}$$

It is worth mentioning that this thermal damage can then result in the blood perfusion change due to the clot or close of blood vessels during magnetic hyperthermia. In general, the blood perfusion coefficient can have different expressions in different variation range, as follows:[41]

$$\omega_b(\Omega) = \begin{cases} \omega_{b0}, & \text{for } \Omega = 0, \\ (1+25\Omega-260\Omega^2)\omega_{b0}, & \text{for } 0<\Omega\le 0.1, \\ (1-\Omega)\omega_{b0}, & \text{for } 0.1<\Omega\le 1, \\ 0, & \text{for } \Omega>1. \end{cases} \tag{23}$$

In addition, the thermal damage due to hyperthermia can further result in the tissue deformation during therapy, which can be understood by the porosity change. This phenomenon can be illustrated by the following expression according to previous literature:[19]

$$\phi' = \phi + (80\% - \phi)(1 - e^{-\Omega(t)}). \tag{24}$$

Further, proper initial and boundary conditions should be also proposed for Eq. (19) in order to obtain the treatment temperature distribution for the proposed model. The initial temperature values for all bio-tissue are set to the normal body temperature, 37 °C. The boundary temperature between different bio-tissue should the requirement of the heat flux continuity during therapy with the following expression:

$$T_0\big|_\gamma = T_1\big|_\gamma, \tag{25}$$

where γ means the boundary between the liver tissue and the healthy tissue.

2.5. Material properties

This study presents the material properties for the proposed model based on previous literature, which include the parameters for the transport model in Table 1 and for the thermal model in Table 2.

Table 1. Transport properties during the nanofluid injection.[28,42–46]

Parameter	Value
ϕ_0	0.12
K_0 (m^2)	8.9×10^{-13}
ρ (g/ml)	1.0
E (Pa)	3.823×10^4
D_{eff} (m^2/s)	5×10^{-12}
v	0.45
β	0.3
d_c (mm)	0.05
η	-1.73×10^{-7}
d_p (nm)	6
L_{PL} ($cm\cdot mmHg^{-1}\cdot s^{-1}$)	2.8×10^{-7}
P_b (mmHg)	15.6
π_b (mmHg)	20
π_i (mmHg)	15
$S_L\cdot V^{-1}$ (cm^{-1})	200

In particular, Table 1 just presents the material properties for the malignant region in which the transport behavior occurs during the nanofluid injection.

Table 2. Thermal characteristics of biological tissues during the simulation.[2]

Parameter	Tumor	Liver	Blood	Fe_3O_4	Unit
ρ	1060	1030	1050	5180	$kg{\cdot}m^{-3}$
k	0.52	0.51	0.51	40	$W{\cdot}m^{-1}{\cdot}K^{-1}$
c	3540	3871	4180	4000	$J{\cdot}kg^{-1}{\cdot}K^{-1}$
ω_{b0}	4.5×10^{-4}	8.33×10^{-4}	1.39×10^{-2}	–	s^{-1}
Q_{met}	684.2	14414	–	–	$W{\cdot}m^{-3}$
A	1.19×10^{35}	–	–	–	J
E_a	2.32×10^{5}	–	–	–	$J\cdot mol^{-1}$
R_u	8.314	–	–	–	

3. Results and discussion

Although this study proposes a three-dimensional model for liver tissue based on a real case, it should not have a better presentation in 3D view since the liver tissue is too large with respect to the proposed tumor size. Thus, this study considers a slice view in the xz plane for most of our simulation results, or also a partial enlarged view for the cross-sectional view for the purpose of enhancing readability. The partial differential equations presented in Section 2 are solved by considering the finite element method for the proposed model, which consists of the nanofluid concentration and also the treatment temperature. The total elements in the proposed three-dimensional model are 12787 with 2610 boundary elements, which result in 20525 freedom degrees for the concentration field and 22475 freedom degrees for the treatment temperature field during the simulation process.

3.1. Fluid distribution field due to the nanofluid injection

In this simulation, the nanofluid for the dose of 0.144 ml is injected into tumor region under the flow rate of 0.06 ml/s before an applied magnetic field works during therapy. Thus, this process will be completed after 2.4 s of nanofluid injection under this specific condition, which can result in the velocity variation inside bio-tissue due to the nanofluid injection. Figure 2 presents the slice view for nanofluid velocity distribution in a logarithmic scale inside tumor region at four different time points, in which the red lines represent the contour line with the logarithm of velocity, -5. As shown in Fig. 2, the maximum velocity appears in the needle tip and keeps unchanged at different stages, which is credited to the constant velocity in the needle tip during the nanofluid injection. Furthermore, one can notice that the area contained in the contour increases with the injection progress.

Nevertheless, there are still a slight difference in the minimum value of velocity at different stages. As can be seen more clearly in Fig. 3, the velocities are the same near the injection site while have a slight difference away from the injection site. The velocity can increase slightly with the injection time at the same location of tumor region.

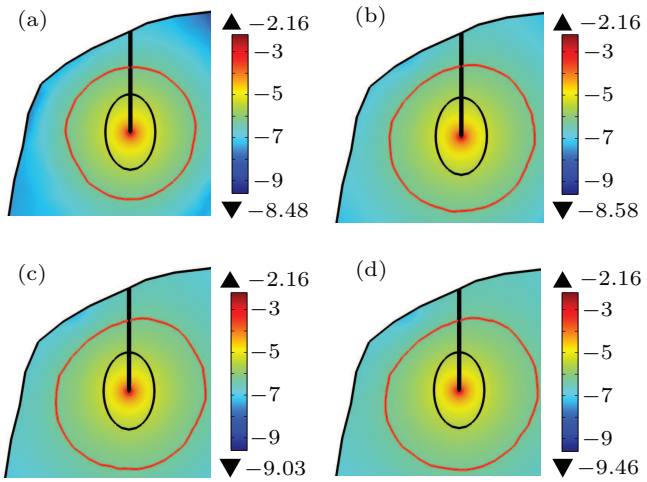


Fig. 2. Velocity distribution in a logarithmic scale at different injection stages: (a) 0.6 s; (b) 1.2 s; (c) 1.8 s; (d) 2.4 s. Velocity is in units of $m{\cdot}s^{-1}$.

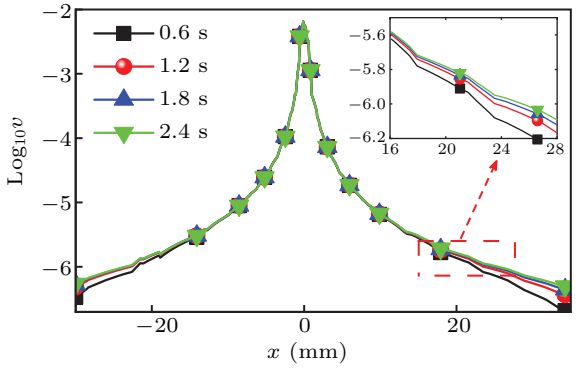


Fig. 3. Logarithm value of velocity for the tumor centerline along x-axis.

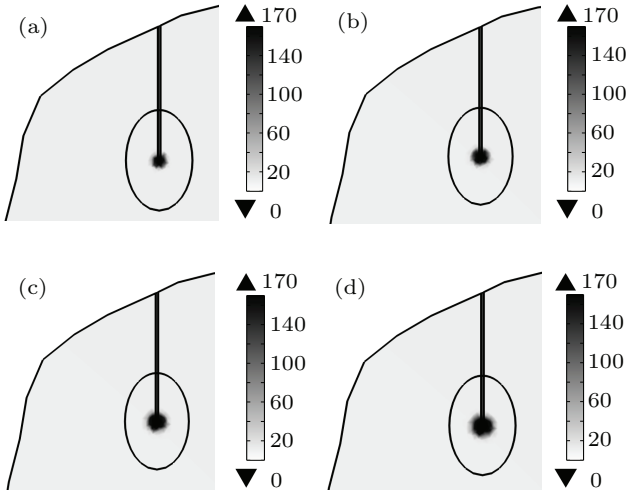


Fig. 4. Concentration distribution for nanofluid injection process at four different time points: (a) 0.6 s; (b) 1.2 s; (c) 1.8 s; (d) 2.4 s. Concentrations are in units of $mg{\cdot}ml^{-1}$.

Further, the nanofluid concentration will also change with the increase of injection duration. Figure 4 presents the slice view for nanofluid spatial distribution inside the tumor region at four different time points during the injection process. As

can be seen, the distribution area of nanofluid increases gradually with the injection duration while the maximum value keeps the same for all time points.

In order to have a better presentation, Fig. 5 describes the nanofluid concentration value for the tumor centerline along x-axis. The diffusion radii in Fig. 5 increase in proportion to the injection duration, which improves from about 6 mm in 0.6 s to 9 mm in 2.4 s of injection duration during injection process. In addition, the concentration value also grows with the injection duration at the same point of nanofluid distribution area.

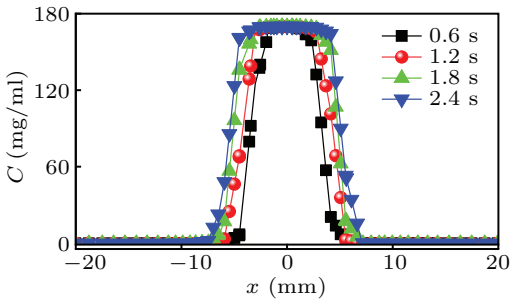


Fig. 5. Concentration values for the tumor centerline along x-axis.

3.2. Tissue deformation due to the nanofluid injection

The nanofluid injection behavior can result in the bio-tissue deformation due to the change in the interstitial pressure inside the tumor region. As can be seen from Fig. 6, the interstitial pressure has the similar characteristics to the velocity and concentration distribution, which also has the maximum value at the needle tip and obtains an increasing area with the injection dose. The red contour lines with a constant log value, 2, illustrate the pressure transfer inside the bio-tissue during injection. Figure 7 presents the interstitial pressure for tumor centerline along x-axis inside the tumor region, in which the logarithm value is considered in both Figs. 6 and 7 in order to have a better presentation. As shown in Fig. 7, although the pressure inside bio-tissue is inversely proportion to the distance away from the injection site, different scenarios still have their discrepancies, especially outside the tumor edge.

The interstitial pressure can also result in the tissue deformation inside bio-tissue, which can be understood by using tissue displacement during the nanofluid injection, as illustrated in Fig. 8. As presented in Fig. 8, the tissue deformation mainly focuses on the bottom tumor of right half and the righthand side of liver region, which depends mostly on the injection site and the nanofluid flow direction. Further, one can also learn from Fig. 8 that the total area of tissue deformation increases gradually with the time-dependent injection dose while the maximum value keeps unchanged at 0.03×10^{-3} m during the entire process. Figure 9 illustrates clearly that the tissue deformation mainly occurs at the injection center, then has a short drop near the injection center and finally decreases gradually from the injection center.

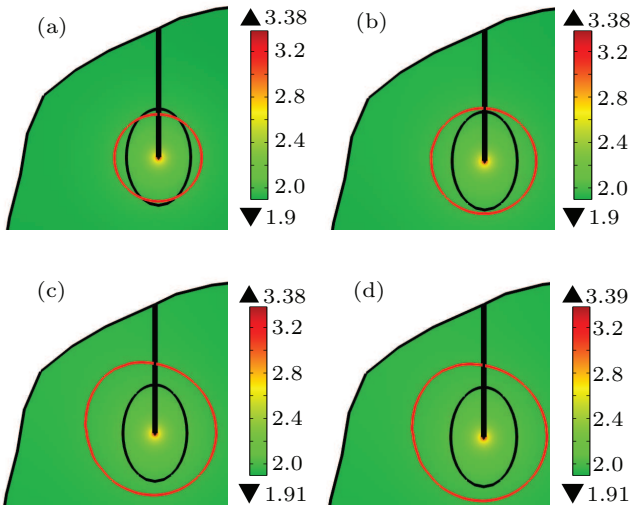


Fig. 6. Logarithm value of pressure distribution for nanofluid injection process at four different time points: (a) 0.6 s; (b) 1.2 s; (c) 1.8 s; (d) 2.4 s.

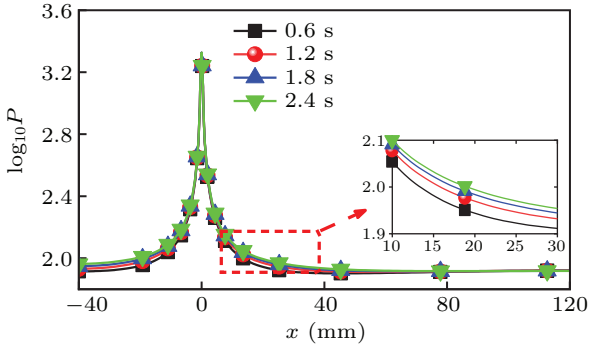


Fig. 7. Logarithm value of pressure for the tumor centerline along x-axis at different injection time.

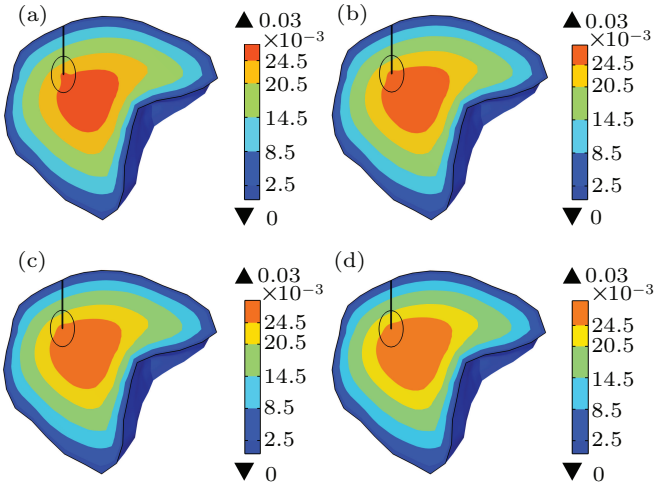


Fig. 8. Tissue displacement distribution at different injection stages: (a) 0.6 s; (b)1.2 s; (c) 1.8 s; (d) 2.4 s.

Furthermore, it is worth mentioning that the injection behavior can change not only the tissue displacement but also other parameter properties, such as the porosity and the permeability of bio-tissue. Figure 10 illustrates the change of parameter properties for tumor centerline at different injection stages, which consists of the porosity and the permeability of bio-tissue. As shown in Fig. 10, the tissue deformation due to the injection behavior results in the increase of tissue porosity

from 12×10^{-2} to 12.53×10^{-2} and the increase of permeability from 8.90×10^{-13} m^2 to 10.12×10^{-13} m^2. Although the change in tissue porosity is not very obvious, the permeability increases by 13.7% since it is the third power relationship of tissue porosity according to Eq. (8). Thus, the combined action of porosity change and permeability variation can promote the nanofluid flow inside the bio-tissue and ultimately lead to a more uniform distribution of nanofluid for malignant region. Therefore, although the change in porosity is relatively small, it can significantly affect the penetration depth of MNPs and should not be ignored during the nanofluid injection. The trends in these two properties are also consistent with the results by Iordana *et al.*,[17] in which the porosity and permeability also have the maximum value in the injection site and decrease with distance from the injection point.

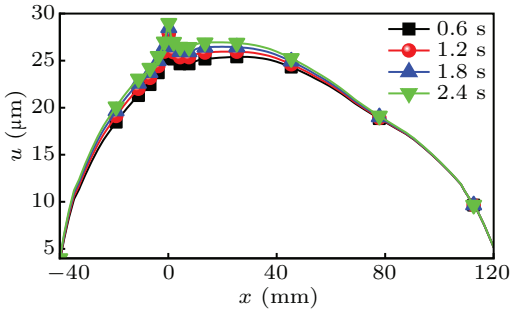


Fig. 9. Tissue displacement for the tumor centerline along x-axis at different injection time.

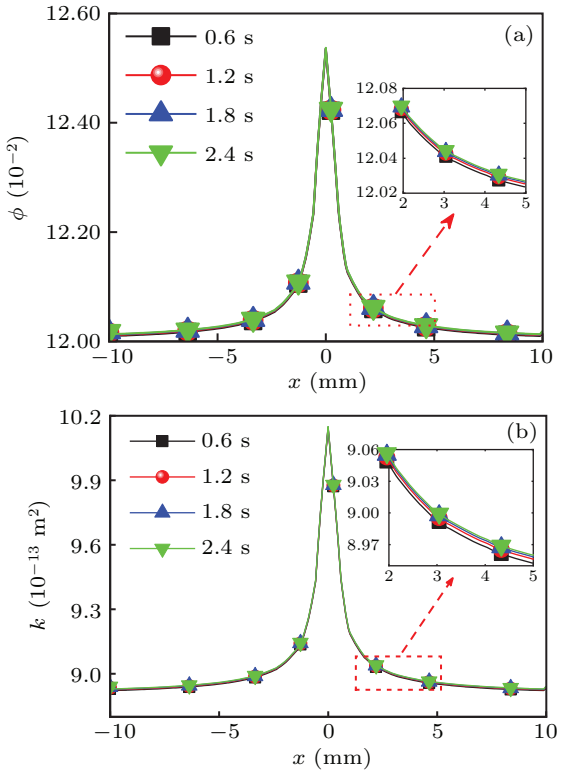


Fig. 10. Variables change for the tumor centerline at different injection stages: (a) porosity; (b) permeability.

Thus, one can conclude that the injection behavior can result in a series of evolutions with the nanofluid injection into bio-tissue, which mainly manifest in the changes in the interstitial pressure, the displacement, the porosity, and the permeability of the tissue. All these changes are normally caused by the increase of interstitial pressure difference inside the bio-tissue due to the injection behavior. The maximum pressure appears in the injection center during the injection process, which also result in the similar situation in the case of the velocity, the concentration, the tissue displacement, the permeability, and the porosity. However, these variations will decrease when far from the injection center, which can be explained by the inverse relationship between the interstitial pressure and the distance away from the injection center. In addition, the tissue displacement can lead to small change in the bio-tissue properties, which mainly consist of the permeability and the porosity. It is worth mentioning that although this study neglects the rebound behavior for the bio-tissue deformation after the nanofluid injection due to its complication, the deformation will gradually decrease with the metabolic time.

3.3. Thermal damage for bio-tissue based on the treatment temperature

The injection behavior should be always accompanied by the nanofluid diffusion during the whole process, which however can be ignored due to its short time injection. Nevertheless, this behavior should be taken into consideration for therapy when the standing time after the injection is long enough. The continuous diffusion time can allow the MNPs to diffuse away from the injection site inside the tumor region due to the difference of interstitial pressure and nanofluid concentration, and ultimately improve the uniformity for nanofluid concentration inside tumor region. Figure 11 illustrates the nanofluid concentration along the tumor centerline after different diffusion time, which are 4 h, 8 h, 12 h, and 16 h, respectively. As can be seen from Fig. 11, the maximum value decreases remarkably with the diffusion duration after the injection while the concentration uniformity for nanofluid obtains a better improvement. The better uniformity in the nanofluid concentration can benefit the treatment effect since it can avoid the local overheating for the therapeutic temperature.

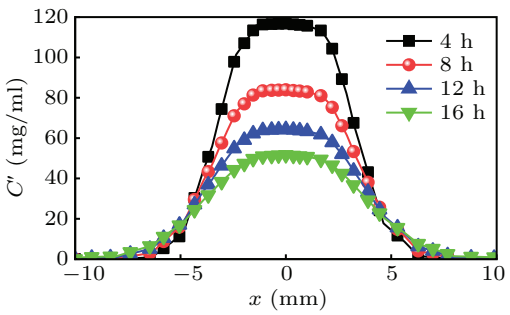


Fig. 11. Nanofluid concentration along the tumor centerline after different diffusion time.

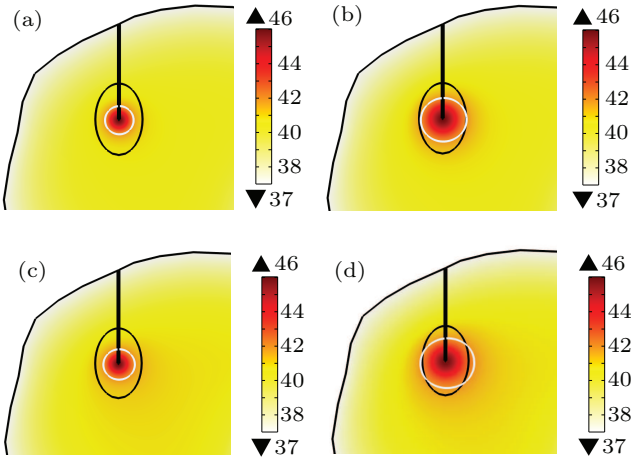


Fig. 12. Treatment temperature distribution for the proposed model in different situations: (a) without diffusion, constant ω_b; (b) after 16 h of diffusion, constant ω_b; (c) without diffusion, variable ω_b; (d) after 16 h of diffusion, variable ω_b.

Although there are many influencing factors for the treatment temperature distribution, the nanofluid concentration distribution is one of the most important item. One can obtain the optimum temperature distribution based concentration distribution when the maximum power dissipation of MNPs is set to a critical value for the proposed model. The optimal situation for the treatment temperature distribution should have a maximum temperature inside the tumor region within a safe value of 46 °C. In addition to the concentration distribution, the blood perfusion rate influenced by the thermal damage should also be taken into consideration according to Eq. (23). In this study, the treatment duration is set to 30 min for safety concerns according to previous literature. This study proposes an evaluating indicator, $L = \iiint \Delta T \, \mathrm{d}v$, in order to estimate the treatment effect for different scenarios, which is the volume integral of the effective temperature increment for the tumor region during the whole treatment. Figure 12 shows the treatment temperature distribution for the proposed model with and without the diffusion behavior and variable blood perfusion rate, in which the white lines indicate the 42 °C contour line for the treatment temperature during magnetic hyperthermia. As illustrated in Fig. 12, the results in Figs. 12(b) and 12(d) have a greater area increment in the temperature distribution with respect to Figs. 12(a) and 12(c), which indicates the diffusion behavior can have an obvious impact on the treatment temperature distribution. Further, there is no significant difference between different cases when the diffusion duration is the same after the nanofluid injection. The volume integral value L in the constant ω_b cases (Figs. 12(a) and 12(b)) are slightly smaller than the cases with a temperature-dependent ω_b (Figs. 12(c) and 12(d)). As illustrated in Fig. 12, the values L are 1.34×10^{-5} in Fig. 12(a) case, 1.66×10^{-5} in Fig. 12(b) case, 1.43×10^{-5} in Fig. 12(c) case, and 1.78×10^{-5} in Fig. 12(d) case, respectively. Thus, one can easily conclude that the treatment temperature distribution will achieve an optimal result for this study when both the temperature-dependent ω_b and nanofluid diffusion are taken into consideration for the simulation. Notably, although the critical power P_{MNP} should be generally different in different scenarios for therapy, it is normally proportional to the uniformity degree of concentration distribution after the nanofluid injection. Thus, the values P_{MNP} in Figs. 12(b) and 12(d) are significantly greater than the value in Figs. 12(a) and 12(c), which are 1.05×10^7 W/m^3 in Fig. 12(b), 9.01×10^6 W/m^3 in Fig. 12(d), 6.4×10^6 W/m^3 in Fig. 12(a), and 5.61×10^6 W/m^3 in Fig. 12(c), respectively. In addition, the critical P_{MNP} can also be different, though the concentration distribution is the same.

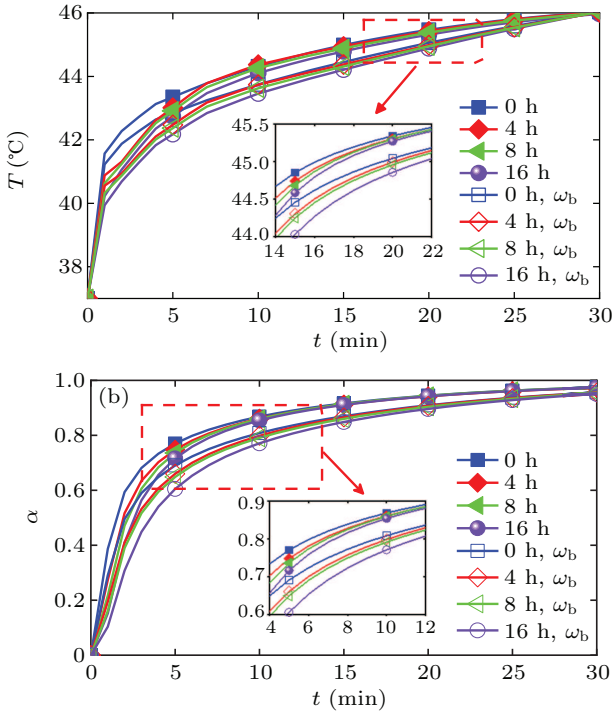


Fig. 13. Different variables change with therapeutic duration for four different cases at the tumor center: (a) temperature; (b) thermal damage degree.

Different scenarios in Fig. 12 should have their individual variation process in the treatment temperature, which will then exhibit different thermal damage for the tumor tissue during therapy. Figure 13 shows the changes of treatment temperature (Fig. 13(a)) and thermal damage degree (Fig. 13(b)) with therapeutic duration for four different cases at the tumor center. As can be seen, the treatment temperature has the fastest rising speed in the constant ω_b case without the diffusion behavior after the nanofluid injection. On the contrary, the treatment temperature with the worst rising speed appears in the variable ω_b case with 16 h of nanofluid diffusion. Thus, the rising speed of treatment temperature is negatively correlated with the nanofluid diffusion time after the injection. On the other hand, the temperature-dependent blood perfusion rate can have a negative influence on the rising speed of temperature with respect to a constant one in this study, which can be

explained by the increase of blood perfusion rate due to thermal damage degree. It is important to note that, the characteristics in the thermal damage degree is positive correlation with the treatment temperature for four different cases presented in Fig. 13(a). However, unlike the treatment temperature, the values of thermal damage degree are different for four different case after 30 min of therapy, which are 0.974, 0.973, 0.956, and 0.950, respectively.

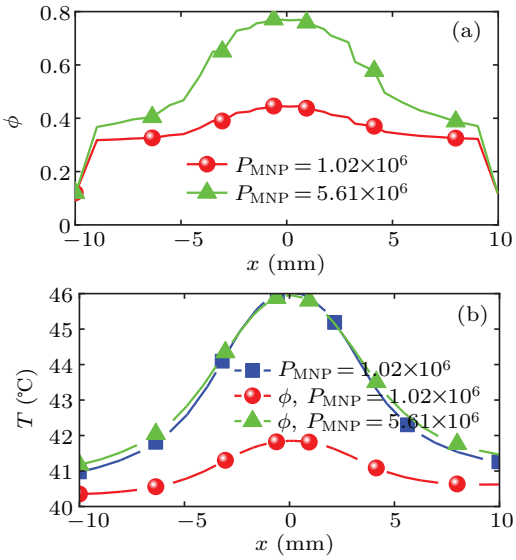


Fig. 14. Effect of power dissipation on different variables along tumor centerline after 30 minutes of treatment: (a) porosity; (b) treatment temperature.

The thermal damage during the therapy can further lead to various degree of tissue deformation when subjected to different treatment conditions including the treatment temperature and the continuous duration. Figure 14(a) presents the change for two different porosities along the tumor centerline under two cases with different power dissipations. The 5.61×10^6 W/m^3 case can have a critical treatment temperature for bio-tissue, in which the porosity is thermal damage-dependent. Alternatively, the heat power in the 1.02×10^6 W/m^3 case can also lead to a critical temperature for therapy when a constant porosity is considered for the simulation. In general, the greater the power dissipation is, the higher the treatment temperature is, and the greater the porosity is, the greater the tissue deformation is. Furthermore, the porosity difference can also result in the difference in the treatment temperature for bio-tissue during therapy. Figure 14(b) shows the change of treatment temperature along the tumor centerline in three different cases. As can be seen, the case considering the tissue deformation can obtain a better treatment effect since the temperature curve receives an overall improvement with respect to the case considering a constant porosity. This situation can also be demonstrated by the proposed evaluating indicator, L, which is improved from 1.3666×10^{-5} to 1.4295×10^{-5} during therapy. However, the case considering a lower P_{MNP}, 1.02×10^6 W/m^3, obtains a worse treatment effect, which is not only reflected in the maximum temperature, 41.8 °C, but also the evaluating indicator, 1.0819×10^{-5}.

4. Conclusions

This study investigates the bio-tissue deformation due to intratumoral injection on magnetic hyperthermia for a proposed three-dimensional liver model. The intratumoral injection can lead to the change in the pressure distribution, the fluid flow rate, the tissue deformation inside the bio-tissue, and ultimately increases the porosity from 12.00×10^{-2} to 12.53×10^{-2} and the permeability from 8.90×10^{-13} m^2 to 10.12×10^{-13} m^2 for the center of bio-tissue. All these variations can directly influence the thermal damage relied on the treatment temperature distribution inside the tumor region, which is significantly determined by the concentration distribution caused by the tissue deformation during the nanofluid injection. The simulation results demonstrate that the treatment temperature distribution for the proposed model appears a better performance when the effect of thermal damage on the blood perfusion rate is taken into consideration, which can be evaluated by the volume integral of the effective temperature increment inside the tumor region. Furthermore, the area for temperature increment can also be improved when the diffusion behavior is considered after the nanofluid injection and an individual critical power is used for therapy. Thus, one can conclude that the treatment effect can be improved by considering nanofluid diffusion, the variable ω_{b}, and also the tissue deformation due to the nanofluid injection during magnetic hyperthermia.

Acknowledgements

Project supported by the National Natural Science Foundation of China (Grant No. 62071124), the Natural Science Foundation of Fujian Province, China (Grant No. 2020J01464), the Education Department of Fujian Province, China (Grant No. JAT190013), and the Conselho Nacional de Desenvolvimento Cientifico e Tecnolóico (BR) (CNPq) (Grant No. 309244/2018-8).

References

[1] Li K, Xu J W, Li P and Fan Y B 2022 *Compos. Pt. B-Eng.* **228** 109401
[2] Astefanoaei I, Dumitru I, Stancu A and Chiriac H 2014 *Chin. Phys. B* **23** 044401
[3] Mona L P, Songca S P and Ajibade P A 2021 *Nanotechnol. Rev.* **11** 176
[4] Tozri A, Alhalafi S, Alrowaili Z A, Horchani M, Omri A, Skini R, Ghorai S, Benali A, Costa B F O and Ildiz G O 2022 *J. Alloys Compd.* **890** 161739
[5] Sokolovskaya O I, Sergeeva E A, Golovan L A, Kashkarov P K, Khilov A V, Kurakina D A, Orlinskaya N Y, Zabotnov S V and Kirillin M Y 2021 *Photonics* **8** 580
[6] Rezanezhad A, Hajalilou A, Eslami F, Parvini E, Abouzari-Lotf E and Aslibeiki B 2021 *J. Mater. Sci. Mater. Electron.* **32** 24026
[7] Tang Y D, Flesch R C C, Jin T and He M H 2021 *Int. J. Heat Mass Transfer.* **178** 121609

[8] Tang Y D, Jin T and Flesch R C C 2017 *IEEE Trans. Magn.* **53** 5400106
[9] Wang Q L and Chen Y Y 2020 *Chin. Phys. B* **29** 084402
[10] Hervault A and Thanh N T K 2014 *Nanoscale* **6** 11553
[11] Zhai Y, Xie H and Gu H 2009 *Int. J. Hyperthermia* **25** 65
[12] Maier-Hauff K, Rothe R, Scholz R, Gneveckow U, Wust P, Thiesen B, Feussner A, von Deimling A, Waldoefner N, Felix R and Jordan A 2007 *J. Neurooncol.* **81** 53
[13] Wu L, Cheng J J, Liu W Z and Chen X G 2015 *IEEE Trans. Magn.* **51** 4600204
[14] Astefanoaei I, Dumitru I, Chiriac H and Stancu A 2014 *IEEE Trans. Magn.* **50** 7400904
[15] Astefanoaei I, Stancu A and Chiriac H 2017 *Eur. Phys. J. Plus* **132** 89
[16] LeBrun A, Manuchehrabadi N, Attaluri A, Wang F, Ma R H and Zhu L 2013 *Int. J. Hyperthermia* **29** 730
[17] Astefanoaei I and Stancu A 2017 *J. Appl. Phys.* **122** 164701
[18] Di Michele F, Pizzichelli G, Mazzolai B and Sinibaldi E 2015 *Math. Biosci.* **262** 105
[19] Singh M, Ma R H and Zhu L 2021 *Int. Commun. Heat Mass Transf.* **126** 105393
[20] Detournay E and Cheng A H D 1993 *Analysis and Design Methods* (Oxford: Pergamon) p. 113
[21] Stoverud K H, Darcis M, Helmig R and Hassanizadeh S M 2012 *Transp. Porous Media* **92** 119
[22] Socrates D 2017 *Modelling Organs, Tissues, Cells and Devices* (Switzerland: Springer) p. 281
[23] Basser P J 1992 *Microvasc. Res.* **44** 143
[24] Chen Z J, Broaddus W C, Viswanathan R R, Raghavan R and Gillies G T 2002 *IEEE Trans. Biomed. Eng.* **49** 85
[25] Hommel J, Coltman E and Class H 2018 *Transp. Porous Media* **124** 589
[26] Netti P A, Baxter L T, Boucher Y, Skalak R and Jain R K 1997 *AICHE J.* **43** 818
[27] Soltani M and Chen P 2011 *PLoS One* **6** e20344
[28] Sefidgar M, Soltani M, Raahemifar K, Bazmara H, Nayinian S M M and Bazargan M 2014 *J. Biol. Eng.* **8** 12
[29] Sefidgar M, Soltani M, Raahemifar K, Sadeghi M, Bazmara H, Bazargan M and Naeenian M M 2015 *Microvasc. Res.* **99** 43
[30] Moghadam M C, Deyranlou A, Sharifi A and Niazmand H 2015 *Microvasc. Res.* **101** 62
[31] Zhang A L, Mi X P, Yang G and Xu L X 2009 *J. Heat Transf. Trans. ASME* **131** 043209
[32] Pizzichelli G, Di Michele F and Sinibaldi E 2016 *Math. Biosci.* **272** 6
[33] Pennes H H 1998 *J. Appl. Physiol.* **85** 5
[34] Rabienejhad M J, Mazaheri A and Davoudi-Darareh M 2021 *Chin. Phys. B* **30** 048401
[35] Li Y Y and Zhang H C 2020 *Chin. Phys. B* **29** 084401
[36] Rosensweig R E 2002 *J. Magn. Magn. Mater.* **252** 370
[37] Li W Y, Li W T, Li B Q, Dong L J, Meng T H, Huo G, Liang G Y and Lu X G 2021 *Chin. Phys. B* **30** 104402
[38] Purdie T G, Lee T Y, Iizuka M and Sherar M D 2000 *Phys. Med. Biol.* **45** 1115
[39] Marek P 2018 *Int. J. Therm. Sci.* **130** 507
[40] Gas P and Wyszkowska J 2019 *Arch. Electr. Eng.* **68** 521
[41] Paruch M 2020 *Materials* **13** 136
[42] Sun J H, Luo Q, Liu L L, Zhang B Y, Shi Y S, Ju Y and Song G B 2016 *J. Biomech.* **49** 45
[43] Wu M, Frieboes H B, McDougall S R, Chaplain M A J, Cristini V and Lowengrub J 2013 *J. Theor. Biol.* **320** 131
[44] Zheng F D, Hou P, Corpstein C D, Xing L and Li T L 2021 *Pharm. Res.* **38** 607
[45] Garcia J J and Smith J 2009 *Ann. Biomed. Eng.* **37** 375
[46] Hou P, Zheng F, Corpstein C D, Xing L and Li T 2021 *Pharm. Res.* **38** 1011